CIWC 2019

sciforum

Conference Proceedings Paper

Corrosion Resistance of Anodic Layers Grown on 304l Stainless Steel at Different Anodizing Times and Stirring Speeds

Laura Patricia Domínguez Jaimes [1], Anabel Álvarez Méndez [1], Astrid Sánchez Vázquez [1], Juan Jacobo Ruiz Valdés [1], Erika Iveth Cedillo González [1], Ana Conde del Campo [2], Juan José De Damborenea González [2], María Ángeles Arenas Vara [2] and Juan Manuel Hernández López [1,*]

[1] Universidad Autónoma de Nuevo León, Facultad de Ciencias Químicas, Ciudad Universitaria, Av. Universidad s/n. C. P. 66455, Nuevo León, México; lauradominguez288@gmail.com (L.P.D.J.); anabel.alvarezmn@uanl.edu.mx (A.A.M.); astrid.sanchezvz@uanl.edu.mx (A.S.V.); juan.ruizv@uanl.mx (J.J.R.V.); erika.cedillogn@uanl.edu.mx (E.I.C.G.)

[2] Department of Surface Engineering Corrosion and Durability, National Center for MetallurgicalResearch, CENIM-CSIC, Avda. Gregorio del Amo, 8, 28040 Madrid, Spain; a.conde@cenim.csic.es (A.C.d.C.); jdambo@cenim.csic.es (J.J.D.G.); geles@cenim.csic.es (M. Á.A.V.)

* Correspondence: hljmanuel@gmail.com or juan.hernandezlz@uanl.edu.mx; Tel.: + 52-1- 55-11941410

Received: 15 February 2019; Accepted: 14 March 2019; Published: 14 March 2019

Abstract: Different chemical and physical treatments have been used to improve the properties and functionalities of steels. The anodizing is one of the most promising treatments, due to its versatility and easy industrial implementation, since it allows obtaining different microstructures on the surface, in order to be employed in different industrial sectors. The present work has studied the influence of the anodizing time (15, 30, 45 and 60 min), as well as the stirring speed (0, 200, 400 and 600 rpm), on the morphology and the resistance corrosion behavior of anodic layers grown in 304L stainless steel. The anodic layers were characterized morphologically, compositionally and electrochemically, in order to determine the influence of these parameters on their corrosion behavior in a 0.6 M NaCl saline solution. The results show that the generation of anodic layers at different times propitiates the definition of nonporous morphologies, while the phenomena of dissolution of the layers that increase with the time of anodizing. However, the resistance to corrosion decreases respect to the non-anodized 304L SS. On the other hand, the effect of the stirring speed during the generation of these anodic layers does not seem to influence the corrosion behavior in the saline medium studied.

Keywords: anodization; stainless steel; anodic layer; corrosion resistance

1. Introduction

In recent years, surface engineering has focused on obtaining physical, chemical, mechanical and microstructural modification treatments on steel, with the purpose of expanding its applications to technological unexplored fields. The range of surface treatments carried out to date is numerous – 6]. Nevertheless, the anodizing process that was initially developed for aluminum [7,8] and later for other metals such as Mg [9], Ga [10], Co [11], W [12], Nb [13], Zr [14], Sn [15], Ti [16,17], it has emerged as a new alternative to the superficial functionalization of iron and its alloys, generating of particular interest in photocatalysis, sensors, corrosion, environmental remediation, biomedical fields, etc. [18–30].

In photocatalysis applications, anodic layers have been considered a suitable way to achieve larger enhancement of surface area. First studies about semiconducting properties and growth of nanostructured layers on ferrous materials were reported by Prakasam et al. [31] who obtained thicknesses of 300–600 nm and pore diameters range from 50 to 250 nm on iron. Further, Zhang et al. has explored the photocatalytic decomposition of methylene blue [19] and the degradation of azo dye [20] by anodic iron oxides in different nanostructures.

Likewise, the nanostructures growth on iron and its alloys show great promise for water splitting reaction under solar or visible-light illumination [23,24]. Rangaraju et al. [25] studied different nanostructure configurations of photoanodes based on anodic iron oxide for photoelectrochemical water oxidation and they obtained better photocatalytic properties in 1 M KOH with AM 1.5 light illumination when the photoanode result in a two-layered oxide structure, a top layer of nano-dendrite morphology and a bottom layer of nanoporous morphology. Also, these same authors affirm that layer next to the metal substrate imparted corrosion resistance compared with a top layer [26].

On the other hand, in terms of biomedical applications, Asoh et al. [29] reported the growth of anodic layers on type 304 stainless steel using hydrogen peroxide and sulfuric acid that work as a highly suitable host for synthetic hydroxyapatite coating to improve bioactivity in biomedical implant devices; and although corrosion resistance is an important issue in medical devices and applications [32,33] and in other industrial applications, the literature is scarce in the electrochemical characterization of anodic layers on stainless steel.

The range of applications depends on the properties, which can be a tailor and improved by manipulating its nanostructure. Moreover, the morphology and structural characteristics of the anodic layers can be deeply correlated with the anodizing conditions. Controlling parameters such as potential applied, temperature, electrolyte composition and anodizing time is key to the formation of anodic layers [18,34–36].

Various researchers have ventured into the growth of anodic layers on stainless steels, with 316L [25,26] and 304 [27–30] being the most commonly used. The studies on 316L SS indicate that in organic solutions the addition of water improves the diameter and thickness of the grown layers [37]. In addition, the use of fluoride-free solutions makes it possible to obtain anodic layers composed of a mixture of hydroxides-oxides-sulphates [38]. However, the growth on stainless steel 304 preferentially made in organic media of glycerol or ethylene glycol with NH_4F and different additions of H_2O, conclude three main points: (1) that the layers have similar Fe, Cr, Ni concentrations of substrate [39]; (2) that the H_2O concentration in the anodized solution determines the morphological characteristics of the anodic layers [40]; and (3) that depending on the voltage applied, different growth mechanisms are favored, leading to the generation of anodic layers with different chemical compositions [29].

Nevertheless, most of the existing works so far are focused on the growth and chemical/ morphological characterization of the anodic layers on these ferrous materials [29,35,39–42], but not in the electrochemical degradation to which these materials may be subjected . For that reason, the objective of this work is to explore the corrosion electrochemical response of anodic layers grown on 304L SS at different stirring speeds and anodizing time using an ethylene glycol–0.1 M NH_4F–0.1 M H_2O electrolyte, in order to be able to glimpse what would be its behavior in chlorides rich solutions.

2. Materials and Methods

Samples of 304L SS with a nominal composition (wt.%) of: 18.3% Cr, 8.11% Ni, 1.52% Mn, 0.27% Si), were ground using successive grades of SiC paper up to 2000 grade, degreased with detergent and rinsed with tap water followed by deionized water.

Anodic layers were formed in a two-electrode cell by anodizing the specimens at constant voltage at 50 V in the electrolyte containing 0.1 M H_2O, 0.1 M NH_4F and ethylene glycol for 15, 30, 45 and 60 min at a constant temperature of 5 °C with uniform stirring and platinum mesh was used as

cathode. Likewise, anodic layers were grown for 15 min, under the afore- mentioned conditions, modifying the agitation of the solution at 0, 200, 400 and 600 rpm.

Plan view morphology of oxide films was examined by field emission gun scanning electron microscopy (FEG–SEM) utilizing JSM6500F JEOL instrument (JEOL, Tokyo, Japan) equipped with EDX facilities, operated at 15 keV for EDX analysis and 7 keV for secondary electron imaging. Each of the area and local EDX analysis results are quoted as an average of 3 measurements.

The electrochemical measurements were done in triplicate in a conventional three-electrode cell. The working electrodes were the non-anodized and anodized samples, an Ag/AgCl electrode (3 M), was used as reference electrode and the counter electrode was a platinum wire. The electrolyte was a 0.6 M NaCl at room temperature. Corrosion behavior was evaluated by potentiodynamic polarization using a Gamry Reference 600 potentiostat (Gamry Instruments, Warminster, PA, USA). The potentiodynamic curves were conducted at a scan rate of 0.16 mV/s. Before starting the scan, the sample remained in the solution for 15 min to stabilize the open circuit potential (OCP). The potential scan was started in the anodic direction from a potential value of 0.3 V with respect to the OCP to 1 V with respect to the Ag/AgCl electrode or when the sample reached a current density of 0.5 A/cm^2.

3. Results and Discussion

3.1. Influence of Stirring Speed on the Growth of Anodic Layers

To investigate the effect of the stirring speed on the growth of the layers, anodized at 4 different stirring speeds (0, 200, 400, 600 rpm) were performed. Figure 1 shows the curves of current density as a function of time recorded during the anodizing treatments. The shape of the potentiostatic curve is typical in the formation of porous morphology anodic layers reported for different valve metals [19, 43–45] and it comprises three stages: (I) an accelerated decrease in the current density during the first seconds of the process, related with the growth of a barrier layer on the surface of the material; (II) a gradual increase of the current density associated with the generation of preferential dissolution zones randomly on the surface of the initial layer; and (III) a stability of the current density related to the growth/dissolution of the anodic layer [46].

Moreover, the charge density that passes through the system during the different treatments at 0, 200, 400 and 600 rpm for 15 min is ~0.750, ~0.864, ~1.027 and ~1.061 C/cm^2, respectively. As from 400 rpm, the anodized curves present an increase in current density and, consequently, in the charge density that may be associated with a greater transport of ionic species from the solution to the metal/electrolyte interface and the acceleration of the chemical dissolution mechanism on the layer as has been reported for the growth of anodic layers on other metallic materials [47,48].

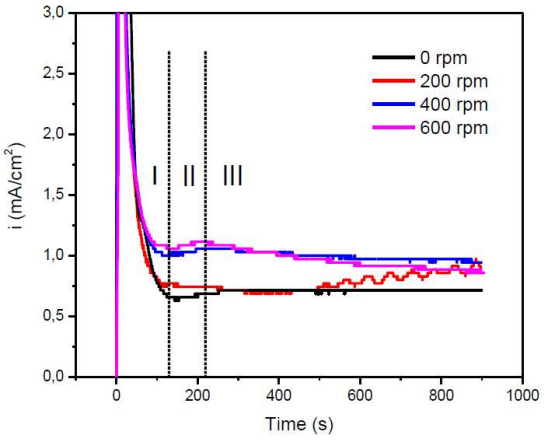

Figure 1. Current density–time responses for anodizing on 304L SS in ethylene glycol-NH_4F-H_2O electrolyte with different stirring speeds.

The electrochemical response was studied by polarization curves in 0.6 M NaCl solution, Figure 2. The non-anodized 304L SS substrate present a corrosion potential (E_{corr}) of ~110.2 mV vs. Ag/AgCl (3 M), a pitting potential (E_{pit}) of ~834.2 mV vs. Ag/AgCl (3 M) and a passive current density (i_{pass}) of 7.71x10^{-8} A/cm^2. On the other hand, the anodic layers showed an unfavorable electrochemical response against corrosion with respect to the substrate, since the E_{corr} was moved to values close to -312.1 mV vs. Ag/AgCl (3 M) while the E_{pit} decreased to ~329.5 mV vs. Ag/AgCl (3 M). Nevertheless, the layer grown at 600 rpm had a much lower pitting potential, with a value of ~140.5 mV vs. Ag/AgCl (3 M), indicating that it is more prone to localized corrosion. In addition, the polarization curves of the anodizing treatments showed narrower passive regions and i_{pass} values around 4.10 × 10^{-7} A/cm^2, which indicates that the layers grown have less corrosion resistance due to the density of passivation increased approximately one order of magnitude compared to the non-anodized sample.

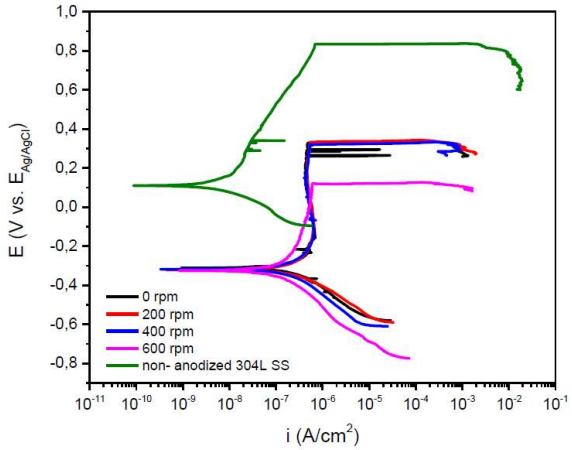

Figure. 2. Potentiodynamic polarization curves of the samples anodized for different stirring speeds.

3.2. Influence of Anodizing Time on the Growth of Anodic Layers

Figure 3 shows the current density-time curves recorded during the anodizing treatments in the electrolyte at 0 rpm and constant agitation of 600 rpm for different anodizing times (15, 30, 45, 60 min). The same stages described for anodizing curve at the same time and different stirring speeds are identified, Figure. 1, but the duration of each one varies significantly with the stirring speed.

As shows in Figure 3a, the first stage associated with the formation of the barrier layer occurs up to 500 s for the anodized at 0 rpm, while at 600 rpm (Figure 3b) the mass transfer is favored leading to out this stage in 200 s. As was expected, higher current densities were observed during the anodization performed in the agitated electrolyte. This increase is also reflected in the charge density, which rose to 4 times its value for the same anodizing time, going from ~0.810 to ~3.626 C/cm^2 for 15 min and from ~1.031 to ~4.438 for 60 min.

The charge density values obtained allow to estimate a theoretical thickness of the anodic layer assuming that the entire charge is used for the formation of FeOOH, which the literature mentions as the main component of the anodic layers grown in ferrous materials [35, 41, 49], obtaining thicknesses of compact amorphous FeOOH of 581 nm (15 min), 1.07 μm (30 min), 1.83 μm (45 min) and 2.60 μm (60 min) at 0 rpm; and 739 nm (15 min), 1.43 μm (30 min), 2.27 μm (45 min) and 3.18 μm (60 min) at 600 rpm. The above could indicate that to greater anodizing time and greater stirring speed would be obtaining thicker anodic layers; however, this approach does not contemplate the processes of chemical dissolution or dissolution assisted by the electric field during the generation of the anodic layers, which results in oxide layers with less thickness [42,50].

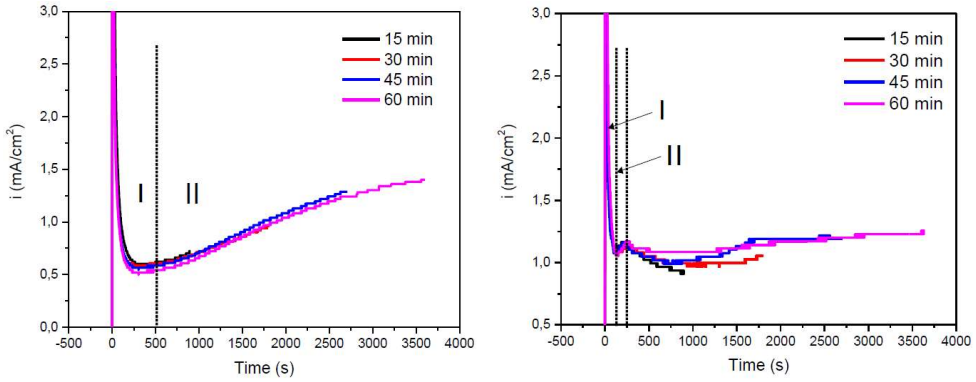

Figure 3. Current density–time responses for anodizing on 304L SS in ethylene glycol-NH_4F-H_2O electrolyte for different anodizing time at (**a**) 0 rpm and (**b**) 600 rpm stirring speeds.

SEM images in Figure. 4 show the morphology evolution of the anodic layers during their growth for different treatment times (15–60 min) at 0 rpm. The anodized layers grown for 15 min show a surface covered with a uniform oxide layer. The beginning of the formation of nanostructures can be observed by the random appearance of pores due to the distribution of the electric field in the anodic layer (Figure 4a,b). After 30 min, rupture of the layer anodic is observed by the appearance of small cracks in the surface associated with its growth and the dissolution of the pores walls (Figure 4c,d) similar to the growth of oxide films on Ti reported by Concha et al. [51]. This behavior is accentuated at 45 min where the cracks become larger and deeper; as a consequence, pore diameters increase and lose definition, varying the diameter from 43.47 ± 6.12 for 30 min to 62.23 ± 12.73 nm for 45 min of treatment, Figure 4e,f.

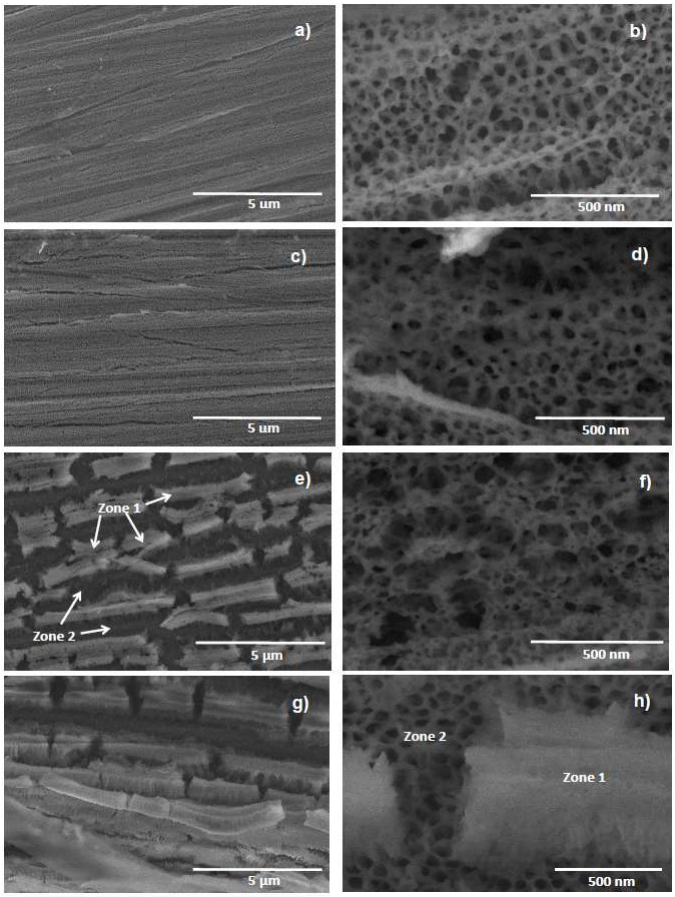

Figure 4. SEM images of anodic layers grown in ethylene glycol-NH_4F-H_2O electrolyte without stirring for (**a**,**b**) 15 min, (**c**,**d**) 30 min, (**e**,**f**) 45 min and (**g**,**h**) 60 min.

The increase of anodizing time to 60 min shows the collapse of outer porous structures giving rise to an ordered pattern of nanostructures in the lower anodic layer, which remains adhered to the substrate (Figure 4g,h). This outer layer (Zone 1) has a thickness of approximately 500 nm. These results reveal that the anodizing time controls both the morphology and the pore diameter, obtaining values of 42.56 ± 5.03 at 15 min and 63.0 ± 11.0 nm at 60 min for anodizing.

On the other hand, Figure 5a shows the results of EDS analysis for anodic layer obtained at 0 rpm for different time of treatment. The distribution of the elements is analyzed in two zones: zone 1 corresponds to the outer layer located at the oxide/electrolyte interface; and zone 2 corresponds to the nanoporous layer adhered to the substrate that is observed after 45 min of treatment, Figure 5b. Both zones show a similar trend since the content of F and O elemental increases while the percentage of other elements such as Cr, Fe and Ni tends to decrease with the time of the anodizing process .The above is caused by a fluorine and oxygen enrichment from the electrolyte, which leads to the formation of fluoride compounds, mainly FeF_2, FeF_3 and FeOOH [40,49].

a)

	Element	C	O	F	Cr	Mn	Fe	Ni
Time	15 min	4.82	5.60	33.77	11.79	0.62	39.34	4.05
	30 min	5.22	8.40	44.68	9.36	0.59	28.99	2.76
	45 min (Zone 1)	3.35	12.53	52.69	8.45	0.24	21.12	1.61
	45 min (Zone 2)	5.93	4.53	17.34	15.27	0.63	50.88	5.41
	60 min (Zone 1)	3.18	22.74	59.06	5.69	0.34	6.86	0.32
	60 min (Zone 2)	8.70	5.21	16.54	14.39	1.35	47.77	6.05

b)

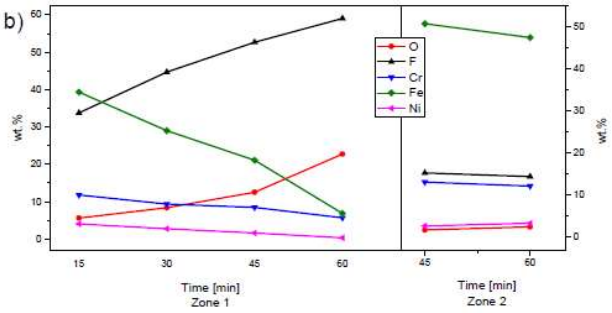

Figure 5. (**a**) EDS results and (**b**) distribution of main elements on the anodic layers for different anodizing times at 0 rpm.

Nevertheless, at 45 min of treatment, F values decrease abruptly from 52.69% to 17.34% and O values from 12.53% to 4.53% between zone 1 and zone 2, respectively. This suggests the possible presence of an immobile C–O layer that limits the migration of ionic species within the anodic layer [50] as reported in previous works on anodic layers grown on Mg using a glycerol-based electrolyte containing 0.35 M NH_4F and 5 vol.% H_2O. The presence of the immobile layer would explain the decrease of anions in zone 2 and the cations in zone 1.

The corrosion behavior of the anodic layers is shown in Figure. 6. The polarization curve for anodizing at 15 min shows a wider passive region compared to the other treatments with a E_{corr} of ~−322.8 mV vs. Ag/AgCl (3 M), lower than the average of the other curves, ~−57.3 mV vs. Ag/AgCl (3 M). However, all treatments show a i_{pass} around ~5.4 × 10^{-7} A/cm^2 and a E_{pit} of ~281.3 mV vs. Ag/AgCl (3 M) indicating a lower corrosion resistance compared to the substrate non-anodized. Performing of a thermal treatment could be an alternative to improve the electrochemical response

of the oxide layers since it allows the obtaining of more stable oxides and the elimination of fluoride inside the anodic layers as they have reported it for layers of Titanium and its alloys [52].

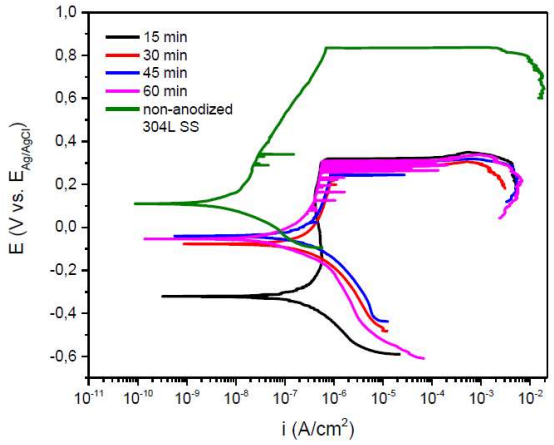

Figure 6. Potentiodynamic polarization curves of the samples anodized for different anodizing times.

4. Conclusions

Anodic layers nano-structured are obtained on 304L SS using ethylene glycol–0.1 M H_2O–0.1 M NH_4F at different stirring speeds and anodizing times. Increasing the stirring speed results in a higher current density response and, as a consequence, an increase in the charge that passes through the system, which is used for the growth of the anodic layers, as well as, in the processes of chemical dissolution and dissolution assisted by the electric field. The increase in anodizing time favors the obtaining of oxide layers with more defined morphologies, superior pore diameters (~63.0 nm) and thicknesses around 500 nm. The chemical composition reveals that exist a dependency with the anodizing time associated with the phenomena of dissolution and migration through the anodic layer, where after 45 min of treatment, a higher content of F and O is identified in the outer zone of the anodic layer. However, the electrochemical responses of the layers grown for all conditions exhibited a less passive and analogous behavior among them. This result is a direct consequence of the high presence of fluoride compounds in the anodic layer that induces a lower corrosion resistance by approximately one order of magnitude with respect to the non-anodized 304L SS substrate.

Conflicts of interest: The authors declare that they do not have any conflicts of interests.

References

1. Jiang, L., J.A. Syed, Y. Gao, H. Lu, and X. Meng, Electrodeposition of $Ni(OH)_2$ reinforced polyaniline coating for corrosion protection of 304 stainless steel. *Applied Surface Science* **2018**, *440*, 1011–1021, doi:10.1016/j.apsusc.2018.01.145.
2. Cano, E., L. Martínez, J. Simancas, F.J. Pérez-Trujillo, C. Gómez, and J.M. Bastidas, Influence of N, Ar and Si ion implantation on the passive layer and corrosion behaviour of AISI 304 and 430 stainless steels. *Surface and Coatings Technology* **2006**, *200*, 5123–5131, doi:10.1016/j.surfcoat.2005.05.029.
3. Dadfar, M., M. Salehi, M.A. Golozar, S. Trasatti, and M.P. Casaletto, Surface and corrosion properties of modified passive layer on 304 stainless steel as bipolar plates for PEMFCs. *International Journal of Hydrogen Energy* **2017**, *42*, 25869–25876, doi:10.1016/j.ijhydene.2017.08.169.
4. García-Rodríguez, S., A.J. López, B. Torres, and J. Rams, 316L stainless steel coatings on ZE41 magnesium alloy using HVOF thermal spray for corrosion protection. *Surface and Coatings Technology* **2016**, *287*, 9–19, doi:10.1016/j.surfcoat.2015.12.075.
5. Habibi, M., S. Javadi, and M. Ghoranneviss, Investigation on the structural properties and corrosion inhibition of W coatings on stainless steel AISI 304 using PF device. *Surface and Coatings Technology* **2014**, *254*, 112–120, doi:10.1016/j.surfcoat.2014.05.070.
6. Awad, A.M., E.A. Ghazy, S.A. Abo El-Enin, and M.G. Mahmoud, Electropolishing of AISI- 304 stainless

steel for protection against SRB biofilm. *Surface and Coatings Technology* **2012**, *206*, 3165–3172, doi:10.1016/j.surfcoat.2011.11.046.

7. Keller, F., M.S. Hunter, and D.L. Robinson, Structural features of oxide coatings on aluminum. *Journal of the Electrochemical Society* **1953**, *100*, 411–419, doi:10.1149/1.2781142.
8. Lee, W. and S.J. Park, Porous anodic aluminum oxide: Anodization and templated synthesis of functional nanostructures. *Chemical Reviews* **2014**, *114*, 7487–7556, doi:10.1021/cr500002z.
9. Blawert, C., W. Dietzel, E. Ghali, and G. Song, Anodizing treatments for magnesium alloys and their effect on corrosion resistance in various environments. *Advanced Engineering Materials* **2006**, *8*, 511–533, doi:10.1002/adem.200500257.
10. Pandey, B., P.S. Thapa, D.A. Higgins, and T. Ito, Formation of self-organized nanoporous anodic oxide from metallic gallium. *Langmuir* **2012**, *28*, 13705–13711, doi:10.1021/la302672a.
11. Lee, C.Y., K. Lee, and P. Schmuki, Anodic formation of self-organized cobalt oxide nanoporous layers. *Angew Chem Int Ed Engl* **2013**, *52*, 2077–2081, doi:10.1002/anie.201208793.
12. Tsuchiya, H., J.M. Macak, I. Sieber, L. Taveira, A. Ghicov, K. Sirotna, and P. Schmuki, Self- organized porous WO3 formed in NaF electrolytes. *Electrochemistry Communications* **2005**, *7*, 295–298, doi:10.1016/j.elecom.2005.01.003.
13. Sieber, I., H. Hildebrand, A. Friedrich, and P. Schmuki, Formation of self-organized niobium porous oxide on niobium. *Electrochemistry Communications* **2005**, *7*, 97–100, doi:10.1016/j.elecom.2004.11.012.
14. Zhang, L., J. Shao, and Y. Han, Enhanced anodization growth of self-organized ZrO2 nanotubes on nanostructured zirconium. *Surface and Coatings Technology* **2011**, *205*, 2876–2881, doi:10.1016/j.surfcoat.2010.10.058.
15. Zaraska, L., K. Gawlak, D. Gilek, and G.D. Sulka, Electrochemical growth of multisegment nanoporous tin oxide layers by applying periodically changed anodizing potential. *Applied Surface Science* **2018**, *455*, 1005–1009, doi:10.1016/j.apsusc.2018.06.044.
16. Zhou, X., N.T. Nguyen, S. Özkan, and P. Schmuki, Anodic TiO2 nanotube layers: Why does self-organized growth occur - A mini review. *Electrochemistry Communications* **2014**, 46, 157– 162, doi:10.1016/j.elecom.2014.06.021.
17. Regonini, D., A. Satka, A. Jaroenworaluck, D.W.E. Allsopp, C.R. Bowen, and R. Stevens, Factors influencing surface morphology of anodized TiO2 nanotubes. *Electrochimica Acta* **2012**, *74*, 244–253, doi:10.1016/j.electacta.2012.04.076.
18. Xie, K., M. Guo, H. Huang, and Y. Liu, Fabrication of iron oxide nanotube arrays by electrochemical anodization. *Corrosion Science* **2014**, *88*, 66–75, doi:10.1016/j.corsci.2014.07.019.
19. Zhang, Z., M.F. Hossain, and T. Takahashi, Fabrication of shape-controlled α-Fe2O3 nanostructures by sonoelectrochemical anodization for visible light photocatalytic application. *Materials Letters* **2010**, *64*, 435–438, doi:10.1016/j.matlet.2009.10.071.
20. Zhang, Z., M.F. Hossain, and T. Takahashi, Self-assembled hematite (α-Fe2O3) nanotube arrays for photoelectrocatalytic degradation of azo dye under simulated solar light irradiation. *Applied Catalysis B: Environmental* **2010**, *95*, 423–429, doi:10.1016/j.apcatb.2010.01.022.
21. Xie, K., J. Li, Y. Lai, W. Lu, Z.a. Zhang, Y. Liu, L. Zhou, and H. Huang, Highly ordered iron oxide nanotube arrays as electrodes for electrochemical energy storage. *Electrochemistry Communications* **2011**, *13*, 657–660, doi:10.1016/j.elecom.2011.03.040.
22. Jang, J.W. and J.W. Park, Iron oxide nanotube layer fabricated with electrostatic anodization for heterogeneous Fenton like reaction. *J Hazard Mater* **2014**, *273*, 1–6, doi:10.1016/j.jhazmat.2014.03.002.
23. Lee, C.Y., L. Wang, Y. Kado, M.S. Killian, and P. Schmuki, Anodic nanotubular/porous hematite photoanode for solar water splitting: Substantial effect of iron substrate purity. *ChemSusChem* **2014**, *7*, 934–940, doi:10.1002/cssc.201300603.
24. Mohapatra, S.K., S.E. John, S. Banerjee, and M. Misra, Water photooxidation by smooth and ultrathin α-Fe2O3 nanotube arrays. *Chemistry of Materials* **2009**, *21*, 3048–3055, doi:10.1021/cm8030208.
25. Rangaraju, R.R., A. Panday, K.S. Raja, and M. Misra, Nanostructured anodic iron oxide film as photoanode for water oxidation. *Journal of Physics D: Applied Physics* **2009**, *42*, 135303, doi:10.1088/0022-3727/42/13/135303.
26. Rangaraju, R.R., K.S. Raja, A. Panday, and M. Misra, An investigation on room temperature synthesis of vertically oriented arrays of iron oxide nanotubes by anodization of iron. *Electrochimica Acta* **2010**, *55*, 785–793, doi:10.1016/j.electacta.2009.07.012.

27. Lucas-Granados, B., R. Sánchez-Tovar, R.M. Fernández-Domene, and J. García-Antón, Controlled hydrodynamic conditions on the formation of iron oxide nanostructures synthesized by electrochemical anodization: Effect of the electrode rotation speed. *Applied Surface Science* **2017**, *392*, 503–513, doi:10.1016/j.apsusc.2016.09.073.
28. Deng, H., M.-C. Huang, W.-H. Weng, and J.-C. Lin, Photocathodic protection of iron oxide nanotube arrays fabricated on carbon steel. *Surface and Coatings Technology* **2015**, *266*, 183–187, doi:10.1016/j.surfcoat.2015.02.042.
29. Asoh, H., M. Nakatani, and S. Ono, Fabrication of thick nanoporous oxide films on stainless steel via DC anodization and subsequent biofunctionalization. *Surface and Coatings Technology* **2016**, *307*, 441–451, doi:10.1016/j.surfcoat.2016.09.025.
30. Yang, Y., J. Zhou, R. Detsch, N. Taccardi, S. Heise, S. Virtanen, and A.R. Boccaccini, Biodegradable nanostructures: Degradation process and biocompatibility of iron oxide nanostructured arrays. *Mater Sci Eng C Mater Biol Appl* **2018**, *85*, 203–213, doi:10.1016/j.msec.2017.12.021.
31. Prakasam, H.E., O.K. Varghese, M. Paulose, G.K. Mor, and C.A. Grimes, Synthesis and photoelectrochemical properties of nanoporous iron(III) oxide by potentiostatic anodization. *Nanotechnology* **2006**, *17*, 4285–4291, doi:10.1088/0957-4484/17/17/001.
32. Zhong, Z., J. Qin, and J. Ma, Cellulose acetate/hydroxyapatite/chitosan coatings for improved corrosion resistance and bioactivity. *Mater Sci Eng C Mater Biol Appl* **2015**, *49*, 251–255, doi:10.1016/j.msec.2015.01.020.
33. Shayan, M., M. Moradi, A.Y. Plakseychuk, R. Shankar, and Y. Chun, Osteoblast cell response to oxide films formed on nanograin 316L stainless steel obtained by two-dimensional linear plane-strain machining. *Materials Letters* **2016**, *177*, 94–98, doi:10.1016/j.matlet.2016.04.178.
34. Pawlik, A., K. Hnida, R.P. Socha, E. Wiercigroch, K. Małek, and G.D. Sulka, Effects of anodizing conditions and annealing temperature on the morphology and crystalline structure of anodic oxide layers grown on iron. *Applied Surface Science* **2017**, *426*, 1084–1093, doi:10.1016/j.apsusc.2017.07.156.
35. Klimas, V., V. Pakštas, I. Vrublevsky, K. Chernyakova, and A.n. Jagminas, Fabrication and characterization of anodic films onto the type-304 stainless steel in glycerol electrolyte. *The Journal of Physical Chemistry C* **2013**, *117*, 20730–20737, doi:10.1021/jp407028u.
36. Albu, S.P., A. Ghicov, and P. Schmuki, High aspect ratio, self-ordered iron oxide nanopores formed by anodization of Fe in ethylene glycol/NH4F electrolytes. *Physica Status Solidi (RRL).*
- *Rapid Research Letters* **2009**, *3*, 64–66, doi:10.1002/pssr.200802285.
37. Tsuchiya, H., T. Suzumura, Y. Terada, and S. Fujimoto, Formation of self-organized pores on type 316 stainless steel in organic solvents. *Electrochimica Acta* **2012**, *82*, 333–338, doi:10.1016/j.electacta.2012.06.048.
38. Doff, J., P.E. Archibong, G. Jones, E.V. Koroleva, P. Skeldon, and G.E. Thompson, Formation and composition of nanoporous films on 316L stainless steel by pulsed polarization. *Electrochimica Acta* **2011**, *56*, 3225–3237, doi:10.1016/j.electacta.2011.01.038.
39. Kure, K., Y. Konno, E. Tsuji, P. Skeldon, G.E. Thompson, and H. Habazaki, Formation of self- organized nanoporous anodic films on type 304 stainless steel. *Electrochemistry Communications* **2012**, *21*, 1–4, doi:10.1016/j.elecom.2012.05.003.
40. Habazaki, H., K. Shahzad, T. Hiraga, E. Tsuji, and T. Aoki, Formation of self-organized porous anodic films on iron and stainless steels. *ECS Transactions* **2015**, *69*, 211–223, doi:10.1149/06902.0211ecst.
41. Jagminas, A., V. Klimas, K. Mažeika, N. Bernotas, A. Selskis, and G. Niaura, Fabrication of thick gel-like films by anodizing iron in a novel electrolyte based on dimethyl sulfoxide and H2SiF6. *Electrochimica Acta* **2011**, *56*, 5452–5458, doi:10.1016/j.electacta.2011.03.011.
42. Shahzad, K., E. Tsuji, Y. Aoki, S. Nagata, and H. Habazaki, Formation and field-assisted dissolution of anodic films on iron in fluoride-containing organic electrolyte. *Electrochimica Acta* **2015**, *151*, 363–369, doi:10.1016/j.electacta.2014.10.132.
43. Roy, P., S. Berger, and P. Schmuki, TiO2 nanotubes: Synthesis and applications. *Angew Chem Int Ed Engl* **2011**, *50*, 2904–2939, doi:10.1002/anie.201001374.
44. Md Jani, A.M., D. Losic, and N.H. Voelcker, Nanoporous anodic aluminium oxide: Advances in surface engineering and emerging applications. *Progress in Materials Science* **2013**, 58, 636– 704, doi:10.1016/j.pmatsci.2013.01.002.
45. Ghicov, A. and P. Schmuki, Self-ordering electrochemistry: A review on growth and functionality of TiO2 nanotubes and other self-aligned MO(x) structures. *Chemical Communications* **2009**, 2791–2808,

doi:10.1039/b822726h.

46. Ono, S., M. Saito, and H. Asoh, Self-ordering of anodic porous alumina formed in organic acid electrolytes. *Electrochimica Acta* **2005**, *51*, 827–833, doi:10.1016/j.electacta.2005.05.058.
47. Syrek, K., J. Kapusta-Kołodziej, M. Jarosz, and G.D. Sulka, Effect of electrolyte agitation on anodic titanium dioxide (ATO) growth and its photoelectrochemical properties. *Electrochimica Acta* **2015**, *180*, 801–810, doi:10.1016/j.electacta.2015.09.011.
48. Grimes, C.A. and G.K. Mor, *TiO2 Nanotube Arrays: Synthesis, properties, and applications*. 2009, Estados Unidos: Springer.
49. Habazaki, H., Y. Konno, Y. Aoki, P. Skeldon, and G.E. Thompson, Galvanostatic growth of nanoporous anodic films on iron in ammonium fluoride-ethylene glycol electrolytes with different water contents. *Journal of Physical Chemistry C* **2010**, *114*, 18853–18859, doi:10.1021/jp1078136.
50. Hernández-López, J.M., A. Němcová, X.L. Zhong, H. Liu, M.A. Arenas, S.J. Haigh, M.G. Burke, P. Skeldon, and G.E. Thompson, Formation of barrier-type anodic films on ZE41 magnesium alloy in a fluoride/glycerol electrolyte. *Electrochimica Acta* **2014**, *138*, 124–131, doi:10.1016/j.electacta.2014.05.147.
51. Concha, O., I.Castañeda, R. Guardian, A. Marban, D. Mayorga, K. Cuentas, J. Uruchurtu, M. Rincon, and C. Menchaca-Campos, Formation of porous anodic film on titanium in acid Mediap containing fluoride Ions at low over-potentials. *Int. J. Electrochem. Sci.* **2015**, 10, 6175– 6186, doi:10.13140/RG.2.1.1724.3929.
52. Matykina, E., J.M. Hernandez-López, A. Conde, C. Domingo, J.J. de Damborenea, and M.A. Arenas, Morphologies of nanostructured TiO2 doped with F on Ti–6Al–4V alloy. *Electrochimica Acta* **2011**, *56*, 2221–2229, doi:10.1016/j.electacta.2010.11.069.